Density functional approach to the effective interaction between charges within dielectric cavities

2002 J. Phys.: Condens. Matter 14 11981

(http://iopscience.iop.org/0953-8984/14/46/308)

INSTITUTE OF PHYSICS PUBLISHING JOURNAL OF PHYSICS: CONDENSED MATTER

J. Phys.: Condens. Matter **14** (2002) 11981–11997 PII: S0953-8984(02)37894-9

Density functional approach to the effective interaction between charges within dielectric cavities

Rosalind Allen and Jean-Pierre Hansen

Department of Chemistry, University of Cambridge, Lensfield Road, Cambridge CB2 1EW, UK

E-mail: rja22@cam.ac.uk

Received 10 June 2002
Published 8 November 2002
Online at stacks.iop.org/JPhysCM/14/11981

Abstract

A variational approach based on a functional of the polarization charge density at interfaces between different dielectric bodies is used to calculate the energy of electrostatic interaction between two electric charges embedded in either two spherical dielectric cavities or in one spheroidal cavity. An effective, distance-dependent dielectric function is extracted from these results, which is exact within the macroscopic theory of dielectrics. We show that different dielectric functions must be associated with pairs of equally or oppositely charged ions and with pairs of ions in cavities of the same or differing radii.

1. Introduction

Electric polarization effects at the interfaces between bodies of different dielectric permittivities play a very important role in understanding many molecular mechanisms on nanometric scales, such as the solvation of highly charged biomolecules [1–3] and the permeation of ions through channels across membranes [4]. A variational approach to the solution of Poisson's equation with appropriate boundary conditions was recently put forward [5]; this variational formulation is particularly efficient when the dielectric interface is assumed to be sharp, since the polarization charge is then restricted to the surface separating two dielectric media. The method was tested against exact results for simple geometries [5], and applied to the permeation of ion channels [4].

In this paper the same density functional formulation is applied to the problem of the effective interaction between two ions of equal or opposite charges, trapped inside dielectric cavities. The first situation which will be considered is that of two separate spheres of permittivity ε placed in a dielectric medium of permittivity ε', each containing an ion. This simple model may be relevant for globular proteins in aqueous solution containing charged residues buried within them, or for ions trapped inside water-in-oil microemulsions or inside micelles. One objective is to determine rigorously, within macroscopic electrostatics, a 'distance-dependent' effective dielectric function which reproduces the total interaction between the two charges. The model is then extended by considering the situation where

the two spherical cavities coalesce into a single spheroidal cavity, with conservation of the total volume of the two initial cavities. A problem similar to the latter was already addressed by Westheimer and Kirkwood [6] in a somewhat different context.

The paper is organized as follows. The electrostatic functional of the polarization charge density is briefly recalled in section 2, and various analytical and numerical strategies for solving the variational problem are examined. The case of charges inside separate spherical dielectric cavities is considered in section 3, while the effective interaction between two charges within the same spheroidal cavity is determined in section 4. A discussion and concluding remarks are contained in section 5.

2. Variational formulation

Electrostatic problems in which distinct regions of space have different dielectric permittivities, with sharp boundaries between them, are a common feature of coarse-grained models of physical systems, including theories of solvation of macromolecules [1–3] and a recent simplified model of an ion channel through a membrane [4]. The electrostatic potential $\psi(\boldsymbol{r})$ of any system containing polarizable bodies may be described in terms of an 'external' part $\psi_e(\boldsymbol{r})$, due to the ions and other fixed charges in the system, and an 'induced' part $\psi_i(\boldsymbol{r})$, which results from the polarization of the system in response to $\psi_e(\boldsymbol{r})$. The induced potential $\psi_i(\boldsymbol{r})$ may be regarded as being caused by a 'polarization charge density' $\rho_{pol}(\boldsymbol{r})$, which is related to the potential and the dielectric susceptibility $\chi(\boldsymbol{r}) = \varepsilon(\boldsymbol{r}) - 1$, by [7]

$$\rho_{pol}(\boldsymbol{r}) = \varepsilon_0 \boldsymbol{\nabla} \cdot [\chi(\boldsymbol{r})\, \boldsymbol{\nabla}\psi(\boldsymbol{r})]. \tag{1}$$

In the particular case of systems with sharp dielectric interfaces, $\rho_{pol}(\boldsymbol{r})$ exists only at the boundaries between regions of differing dielectric permittivities, apart from a trivial part located at the positions of the external charges $\boldsymbol{r}_q$, $\rho_{triv} = q(1/\varepsilon - 1)\delta(\boldsymbol{r} - \boldsymbol{r}_q)$, which simply has the effect of screening the potential of the point charges by a factor $1/\varepsilon$, where ε is the permittivity of the medium containing the external charges. One may thus describe the total potential of the system by specifying a surface polarization charge density $h(\boldsymbol{s}) = \rho_{pol}(\boldsymbol{s})/\varepsilon_0$.

A variational method for solving such problems was introduced in a previous paper [5]. This consists of a functional $I[h(\boldsymbol{s})]$, defined on the surface separating the dielectric bodies in the system, the minimization of which, with respect to $h(\boldsymbol{s})$, leads to the correct electrostatic solution. $I[h]$ is given by

$$\begin{aligned} I[h] = &-\frac{(\kappa-1)}{2}\int_S \mathrm{d}^2 s \int_S \mathrm{d}^2 s'\, h(\boldsymbol{s}')\frac{\partial G(\boldsymbol{s}-\boldsymbol{s}')}{\partial n}\left[\psi_e(\boldsymbol{s}) + \int_S \mathrm{d}^2 s''\, h(\boldsymbol{s}'')G(\boldsymbol{s}-\boldsymbol{s}'')\right] \\ &+ \frac{(\kappa+1)}{4}\int_S \mathrm{d}^2 s \int_S \mathrm{d}^2 s'\, h(\boldsymbol{s})h(\boldsymbol{s}')G(\boldsymbol{s}-\boldsymbol{s}') \\ &+ \frac{(\kappa-1)}{4}\int_S \mathrm{d}^2 s\, \psi_e(\boldsymbol{s})h(\boldsymbol{s}) - \frac{(\kappa-1)}{2}\int_S \mathrm{d}^2 s \int_S \mathrm{d}^2 s'\, h(\boldsymbol{s}')G(\boldsymbol{s}-\boldsymbol{s}')\frac{\partial \psi_e(\boldsymbol{s})}{\partial n} \end{aligned} \tag{2}$$

where $\kappa = \varepsilon'/\varepsilon$, ($\varepsilon'$ referring to the region not containing the fixed charges), $G(\boldsymbol{r} - \boldsymbol{r}') = 1/(4\pi|\boldsymbol{r} - \boldsymbol{r}'|)$ is the Green function for an infinite system, and $\frac{\partial}{\partial n}$ indicates a derivative in the direction of the normal to the dielectric interface, pointing from region (ε) to region (ε').

$I[h]$ was derived in [5] in the particular case where $\varepsilon = 1$, i.e. the fixed charges were situated in vacuum. However, it may be generalized to cases where $\varepsilon \neq 1$ by using the definition of κ given above and defining the potential of the fixed charges, ψ_e, as

$$\psi_e(\boldsymbol{r}) = \sum_{i=1}^{N} \frac{q_i}{\varepsilon\varepsilon_0} G(|\boldsymbol{r} - \boldsymbol{r}_i|). \tag{3}$$

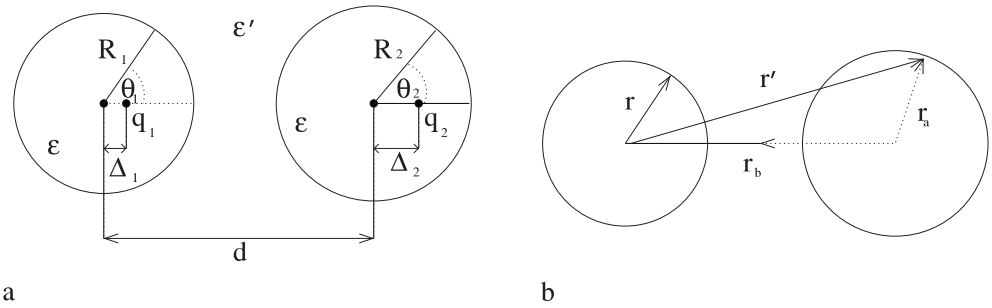

a b

Figure 1. (a) The geometry of the dielectric problem involving two charges (q_1, q_2) embedded in spherical bodies of radii (R_1, R_2) and dielectric permittivity ε, surrounded by a dielectric continuum ε'. (b) A vector diagram showing point $\boldsymbol{r} = (R_1, \theta_1, \phi_1)$ on sphere 1 and point $\boldsymbol{r}' = (r', \theta', \phi')$ on sphere 2, where $\boldsymbol{r}' = \boldsymbol{r}_b - \boldsymbol{r}_a$, with $\boldsymbol{r}_b = (r_b, \theta_b, \phi_b) = (d, \pi, \phi_b)$ and $\boldsymbol{r}_a = (r_a, \theta_a, \phi_a) = (R_2, \theta_2, \phi_2)$.

This variational method was previously applied to several problems in simple geometries, for which $I[h]$ could be minimized both analytically, via an expansion in suitable orthogonal basis functions, and numerically on a surface grid [5]. When solving numerically in this way, it is necessary to make approximations to deal with the divergence of $G(\boldsymbol{r} - \boldsymbol{r}')$ at grid points where $\boldsymbol{r} = \boldsymbol{r}'$. This forms the major source of error in numerical calculations involving large peaks in $h(\boldsymbol{s})$, for example where there are two very closely spaced dielectric boundaries or a very large dielectric discontinuity.

The numerical method has recently been applied in a molecular dynamics simulation of a simple model of a channel through a membrane [4].

Two different electrostatic problems are treated in this work: that of two dielectric spheres, each containing a point charge, and that of two point charges contained within a dielectric spheroid. The latter problem is solved by an expansion of $h(\boldsymbol{s})$ in orthogonal basis functions, followed by an analytical minimization of $I[h]$. However, there is no such set of orthogonal basis functions suitable for the former situation. After an initial approach using grids defined on the two spheres, a numerical method was devised based on a separate expansion of $h(\boldsymbol{s})$ on each sphere, which eliminates the approximations required for the grid-based method. The method is tested against an analytical solution in bispherical coordinates, obtained for a particular configuration of the point charges within the spheres.

3. Charges inside separate dielectric spheres

We first consider two charges, q_1 and q_2, placed a distance d apart and contained within spherical dielectric bodies of permittivity ε, surrounded by a medium of permittivity ε', as shown in figure 1(a). The spheres have radii R_1 and R_2 and the charges may be displaced from the centres of the spheres by distances Δ_1 and Δ_2.

The potential energy of interaction, V_{int}, between the two spheres may be defined as the total energy of the system at distance d, less the polarization energy of each sphere due to its own point charge, measured when the spheres are infinitely far apart (see equation (16)).

At very large d, the spheres do not interact and each one has a surface polarization charge density induced simply by the point charge within that sphere (note that when $\Delta = 0$ this takes the form of a uniform surface charge). In this large-d limit, V_{int} is expected to be of the form $V_{int}(d) = q_1 q_2/(4\pi\varepsilon'\varepsilon_0 d)$. As d decreases, however, each point charge is able to polarize the other sphere as well as its own, leading to a correlation between the polarization surface

charge densities on the two spheres. The interaction energy may be cast into the same form if an 'effective dielectric function', $\varepsilon_{eff}(d)$, is defined such that

$$V_{int}(d) = \frac{q_1 q_2}{4\pi\,\varepsilon_{eff}\varepsilon_0 d}. \tag{4}$$

The function $\varepsilon_{eff}(d)$ includes all polarization interactions between the two spheres. If more than two spherical cavities are present, the electrostatic interaction energy is not expected to be pairwise additive, but three-and more-body interactions come into play. However, a sum of pairwise terms of the form (4) may provide a good first approximation to the total electrostatic interaction energy, at least for dilute dispersions of spherical bodies. An investigation along these lines is under way.

3.1. Variational method

The problem posed above may be solved numerically using the variational functional (2) without the need for a grid spanning the dielectric interface. We define coordinates $(\rho_1, \theta_1, \phi_1)$, centred at $z = -d/2$, and $(\rho_2, \theta_2, \phi_2)$, centred at $z = +d/2$, as shown in figure 1(a). In view of the cylindrical symmetry around the z-axis, the total induced polarization surface charge density is then expanded in Legendre polynomials on the two spherical surfaces:

$$h(\boldsymbol{s}) = h_1(\boldsymbol{s}_1) + h_2(\boldsymbol{s}_2) = \sum_{l=0}^{\infty}[A_l P_l(\cos\theta_1) + B_l P_l(\cos\theta_2)]. \tag{5}$$

The aim is to find the expansion coefficients A_l and B_l.

The Green function between two position vectors $\boldsymbol{r}$ and $\boldsymbol{r}'$ is given in spherical polar coordinates by [7]

$$G(\boldsymbol{r} - \boldsymbol{r}') = \sum_{l=0}^{\infty} \frac{1}{(2l+1)} \frac{\rho_<^l}{\rho_>^{l+1}} \sum_{m=-l}^{l} Y_{lm}^*(\theta, \phi) Y_{lm}(\theta', \phi') \tag{6}$$

where $Y_{lm}(\theta, \phi)$ and $Y_{lm}(\theta', \phi')$ are spherical harmonics having the same origin, and $\rho_<$ and $\rho_>$ are the smaller and larger of the two radial components, $|\boldsymbol{r}|$ and $|\boldsymbol{r}'|$.

The case where $\boldsymbol{r}$ and $\boldsymbol{r}'$ lie on different spheres is illustrated in figure 1(b). The vectors $\boldsymbol{r}'$, $\boldsymbol{r}_a$, and $\boldsymbol{r}_b$, where $\boldsymbol{r}' = \boldsymbol{r}_a - \boldsymbol{r}_b$, as shown in figure 1(b), are related in spherical coordinates by [8]

$$\frac{1}{r'^{l+1}} Y_{lm}(\theta', \phi') = \sqrt{\frac{4\pi}{(2l)!}} \sum_{\lambda=0}^{\infty} (-1)^{l+\lambda} \sqrt{\frac{(2(l+\lambda))!}{(2\lambda+1)!}} \frac{r_a^\lambda}{r_b^{l+\lambda+1}}$$
$$\times \sum_{\mu=-\lambda}^{\lambda} \langle \lambda(l+\lambda)\mu(m+\mu)|lm\rangle Y_{\lambda\mu}(\theta_a, \phi_a) Y_{l+\lambda, m+\mu}(\theta_b, \phi_b) \tag{7}$$

where $\langle \lambda(l+\lambda)\mu(m+\mu)|lm\rangle$ is a Clebsch–Gordan coefficient [9].

Since $\boldsymbol{r}_b$ is the vector between the centres of the two spheres, $\rho_b = d$, $\theta_b = \pi$, and $Y_{l+\lambda, m+\mu}(\theta_b, \phi_b) = (-1)^{(l+\lambda)}(\frac{2(l+\lambda)+1}{4\pi})^{1/2}\delta_{m+\mu,0}$. The Green function between points $\boldsymbol{r}$ on the surface of sphere 1 and $\boldsymbol{r}'$ on the surface of sphere 2, as shown in figure 1(b), may therefore be written as

$$G(\boldsymbol{r} - \boldsymbol{r}') = \sum_{l=0}^{\infty} \frac{1}{(2l+1)} R_1^l \sum_{m=-l}^{l} Y_{lm}^*(\theta_1, \phi_1)$$
$$\times \sqrt{\frac{1}{(2l)!}} \sum_{\lambda=0}^{\infty} \sqrt{\frac{(2(l+\lambda)+1)!}{(2\lambda+1)!}} \frac{R_2^\lambda}{d^{l+\lambda+1}} \langle \lambda(l+\lambda) - m0|lm\rangle Y_{\lambda-m}(\theta_2, \phi_2). \tag{8}$$

The external potential on the dielectric boundary is also expanded in Legendre polynomials:

$$\psi_e(\boldsymbol{s}) = \psi_e^{(1)}(\boldsymbol{s}_1) + \psi_e^{(2)}(\boldsymbol{s}_2) = \frac{1}{4\pi\varepsilon\varepsilon_0}\sum_{l=0}^{\infty}[\Psi_l^{(1)}P_l(\cos\theta_1) + \Psi_l^{(2)}P_l(\cos\theta_2)] \tag{9}$$

where $\Psi_l^{(1)} = q_1\Delta_1^l/R_1^{l+1} + q_2R_1^l/(d+\Delta_2)^{l+1}$ and $\Psi_l^{(2)} = q_2\Delta_2^l/R_2^{l+1} + q_1R_2^l(-1)^l/(d-\Delta_1)^{l+1}$.

The derivative of the external potential, $\partial\psi_e/\partial n = \partial\psi_e/\partial R$, is given by

$$\frac{\partial\psi_e(\boldsymbol{s})}{\partial n} = \frac{1}{4\pi\varepsilon\varepsilon_0}\sum_{l=0}^{\infty}[\Xi_l^{(1)}P_l(\cos\theta_1) + \Xi_l^{(2)}P_l(\cos\theta_2)] \tag{10}$$

where $\Xi_l^{(1)} = -(l+1)q_1\Delta_1^l/R_1^{l+2} + lq_2R_1^{l-1}/(d+\Delta_2)^{l+1}$ and $\Xi_l^{(2)} = -(l+1)q_2\Delta_2^l/R_2^{l+2} + lq_1R_2^{l-1}(-1)^l/(d-\Delta_1)^{l+1}$.

Substituting (5)–(9) into the functional (2), using the orthogonality relations for spherical harmonics [7] as well as the fact that [9]

$$\langle\lambda(l+\lambda)00|l0\rangle = (-1)^{2l+\lambda}(2l+1)^{1/2}\left(\frac{(2\lambda)!(2l)!}{(2(l+\lambda)+1)!}\right)^{1/2}\frac{(l+\lambda)!}{l!\lambda!} \tag{11}$$

the following expression for the functional $I[h]$ is obtained:

$$I[h] = -\frac{(\kappa-1)}{4}[2I^{(1)} + 2I^{(2)} + 2I^{(3)} + I^{(4)}] + \frac{(\kappa+1)}{4}I^{(5)} \tag{12}$$

where $I^{(1)}$ to $I^{(5)}$ are given by

$$I^{(1)} = \frac{R_1^2R_2^2}{\varepsilon}\sum_{l=0}^{\infty}\sum_{n=0}^{\infty}\frac{(-1)^n(n+l)!R_1^lR_2^n}{n!l!(2n+1)(2l+1)d^{l+n+1}}\left[\frac{A_l\Psi_l^{(2)}}{R_2} + \frac{B_l\Psi_l^{(1)}}{R_1}\right] - \frac{1}{2\varepsilon}\sum_{l=0}^{\infty}\frac{[R_1^2A_1\Psi_l^{(1)} + R_2^2B_l\Psi_l^{(2)}]}{(2l+1)^2} \tag{13a}$$

$$I^{(2)} = \frac{R_1^2R_2^2}{\varepsilon}\sum_{l=0}^{\infty}\sum_{n=0}^{\infty}\frac{(-1)^nR_1^lR_2^n(l+n)!}{n!l!(2l+1)(2n+1)d^{l+n+1}}[A_l\Xi_n^{(2)} + \Xi_l^{(1)}B_n] + \frac{1}{\varepsilon}\sum_{l=0}^{\infty}\frac{[R_1^3A_l\Xi_l^{(1)} + R_2^3B_l\Xi_l^{(2)}]}{(2l+1)^2} \tag{13b}$$

$$I^{(3)} = -2\pi\sum_{l=0}^{\infty}\frac{[R_1^3A_l^2 + R_2^3B_l^2]}{(2l+1)^3} + 2\pi R_1^2R_2^2\sum_{l=0}^{\infty}\sum_{n=0}^{\infty}\frac{A_lB_nR_1^lR_2^n(-1)^n(n+l)!}{n!l!(2n+1)(2l+1)d^{l+n+1}}\left[\frac{2n-1}{2n+1} + \frac{2l-1}{2l+1}\right] + 4\pi R_1^3R_2^3\sum_{l=0}^{\infty}\sum_{n=0}^{\infty}\sum_{p=0}^{\infty} \times \frac{p(l+p)!(n+p)![A_lA_nR_1^{l+n}R_2^{2p-1} + (-1)^{l+n}B_lB_nR_2^{l+n}R_1^{2p-1}]}{(2l+1)(2n+1)(2p+1)l!n!(p!)^2d^{2p+l+n+2}} \tag{13c}$$

$$I^{(4)} = \frac{1}{\varepsilon}\sum_{l=0}^{\infty}\frac{[R_1^2A_l\Psi_l^{(1)} + R_2^2B_l\Psi_l^{(2)}]}{(2l+1)} \tag{13d}$$

$$I^{(5)} = 8\pi R_1^2R_2^2\sum_{l=0}^{\infty}\sum_{n=0}^{\infty}\frac{(-1)^nA_lB_n(n+l)!R^lR^n}{(2l+1)(2n+1)n!l!d^{l+n+1}} + 4\pi\sum_{l=0}^{\infty}\frac{[R_1^3A_l^2 + R_2^3B_l^2]}{(2l+1)^2}. \tag{13e}$$

The expansion (5) of the induced polarization surface charge density $h(s)$ is truncated at a finite number N of coefficients; we find $N = 15$ sufficient for convergence. Powell's method [10] is then used to perform a numerical minimization with respect to the coefficients A_n and B_n.

Once A_n and B_n are obtained, the polarization energy V_{pol} is calculated using the relation [7]

$$V_{pol} = \frac{1}{2}\int \mathrm{d}^2 s\, \varepsilon \psi_e(\boldsymbol{s})\rho_{pol}(\boldsymbol{s}) = \frac{1}{2}\sum_{l=0}^{\infty}\frac{[R_1^2\Psi_l^{(1)}A_l + R_2^2\Psi_l^{(2)}B_l]}{(2l+1)}. \tag{14}$$

The total energy V_{tot} is given by

$$V_{tot} = \frac{q_1 q_2}{4\pi\varepsilon\varepsilon_0(d - \Delta_1 + \Delta_2)} + V_{pol}. \tag{15}$$

Note that the factor of ε in (14) is included because of the particular definition of ψ_e in (3): the polarization surface charge interacts with the bare, unscreened, point charges. Interactions of the trivial part of the induced charge, ρ_{triv}, with the opposite point charge are included in the first part of V_{tot}.

The interaction energy was defined above to be

$$V_{int}(d) = V_{tot}(d) - V_{pol}|_{d\to\infty}. \tag{16}$$

The polarization energy is known exactly in the limit of isolated spheres:

$$V_{pol}|_{d\to\infty}(\Delta_1, \Delta_2) = \frac{(\varepsilon - \varepsilon')}{8\pi\varepsilon\varepsilon_0}\sum_{l=0}^{\infty}\frac{1}{\varepsilon l + \varepsilon'(l+1)}\left(\frac{q_1\Delta_1^{2l}}{R_1^{2l+1}} + \frac{q_2\Delta_2^{2l}}{R_2^{2l+1}}\right). \tag{17}$$

When $\Delta_1 = \Delta_2 = 0$ this expression simplifies to $\frac{(\varepsilon-\varepsilon')}{8\pi\varepsilon_0\varepsilon\varepsilon'}\left(\frac{q_1}{R_1} + \frac{q_2}{R_2}\right)$.

We note that this minimization scheme may easily be generalized to the case where there are more than two spheres.

3.2. Testing against an exact solution in bispherical coordinates

The numerical solution obtained by the method illustrated in section 3.1 can be tested against an analytic solution to the problem in the particular geometry where $R_1 = R_2 = R$; $\Delta_1 = -\Delta_2 = \Delta$, obtained within the bispherical coordinate system (μ, η, ϕ) [11]. In this coordinate system, the ϕ-variable has the same meaning as in cylindrical coordinates, and will not concern us here, since our problem is azimuthally symmetric. A surface of constant $\mu = \mu_0$ forms a sphere of radius $R = |a/\sinh\mu_0|$ with its centre positioned at $z = a\coth\mu_0$. Positions on the surface of this sphere are described by the η-coordinate. When $\mu \to \pm\infty$, two points are obtained on the z-axis, at $z = \pm a$.

Bispherical coordinates are well suited to the problem of two point charges (q_1, q_2) located at $z = (-a, +a)$, surrounded by dielectric spheres (here taken to be of equal radius, for simplicity) given by $\mu = (-\mu_0, +\mu_0)$, centred at $z = (-d/2, +d/2) = (-a\coth\mu_0, +a\coth\mu_0)$, as illustrated in figure 2. The detailed solution is given in appendix A. The result of the calculation is an induced charge density on the surface of the two spheres, of the form

$$h^{(1)}(\eta) = (\cosh\mu_0 - \cos\eta)^{1/2}\sum_n Z_n P_n(\cos\eta) \tag{18}$$

$$h^{(2)}(\eta) = (\cosh\mu_0 - \cos\eta)^{1/2}\sum_n W_n P_n(\cos\eta) \tag{19}$$

where the coefficients Z_n and W_n are given in equations (A.16) and (A.17).

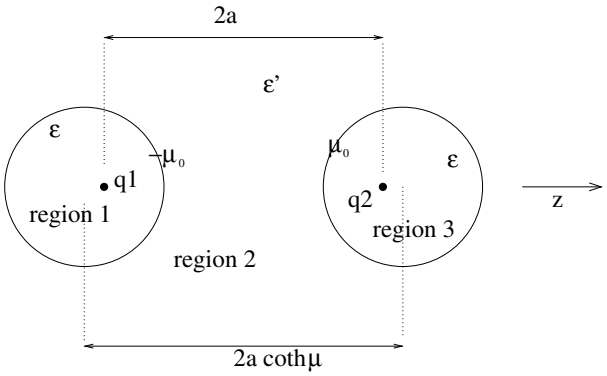

Figure 2. The geometry adopted for the exact solution in bispherical coordinates. The two spheres have radius $R = |a/\sinh\mu_0|$, the charges q_1 and q_2 are positioned at $z = \mp a = \mp(d - \Delta)$, and the centres of the spheres are at $z = \pm a\coth\mu_0 = \pm d/2$.

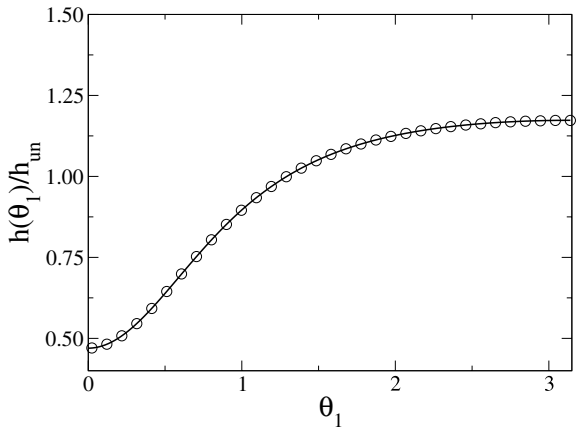

Figure 3. Induced polarization charge density as a function of angle θ_1 (in radians, as defined in figure 1(a)), relative to the value h_{un} for $d \to \infty$ and $\Delta = 0$, $h_{un} = \frac{q}{4\pi R^2\varepsilon_0}(\frac{1}{\varepsilon'} - \frac{1}{\varepsilon})$. Here, $R_1 = R_2 = R$, $d/R = 3$, $q_1 = q_2$, $\varepsilon = 80$, $\varepsilon' = 1$. The point charges are positioned as described in figure 2 and section 3.2. The solid curve shows the results obtained from the calculation in bispherical coordinates and the circles show the numerical minimization results.

The calculation is performed for specified values of d and R, as in figure 1(a), setting the parameters a and μ_0 via $a^2 = (d^2/4) - R^2$ and $\sinh^2\mu_0 + 1 = d^2/(4R^2)$. The numerical minimization described in section 3.1 is then carried out for the same geometry, with $\Delta = \frac{d}{2}[1 - (1 - 4R^2/d^2)^{1/2}]$. The resulting induced polarization charge density is compared to the analytical result, for $\varepsilon = 80$, $\varepsilon' = 1$, and $d/R = 3$ in figure 3. The results of the analytical and numerical methods are seen to agree perfectly.

3.3. Results

Having verified the accuracy of the variational procedure outlined in section 3.1 for solving problems in this geometry, we now apply it to physically relevant situations. These fall into two classes: those in which the material inside the spheres is the more polarizable ($\varepsilon > \varepsilon'$),

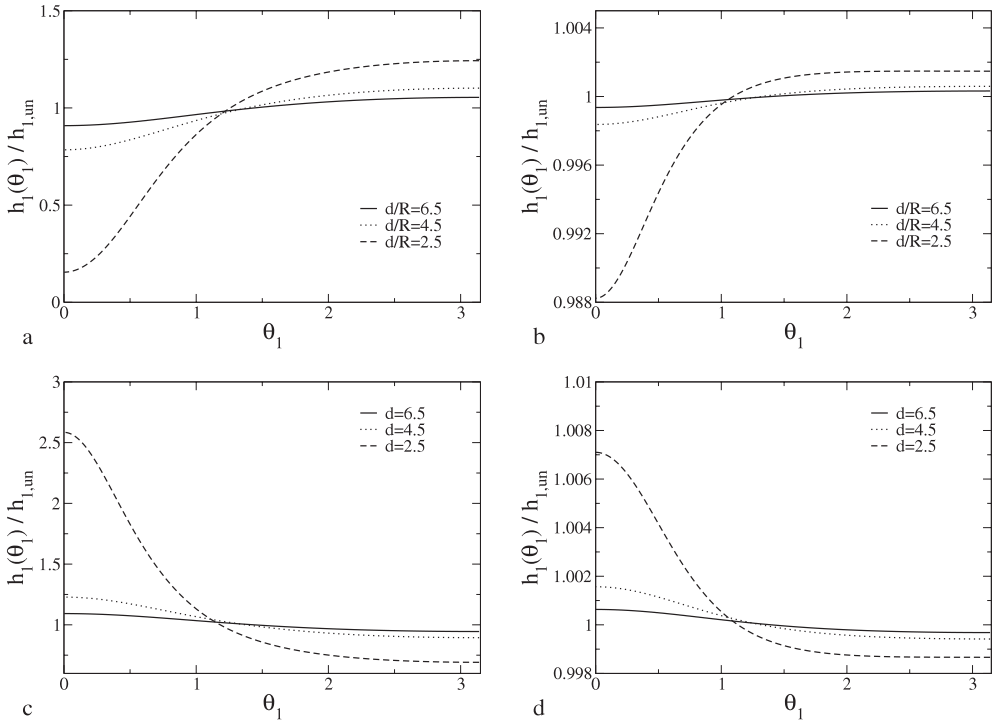

Figure 4. Induced polarization surface charge density on sphere 1 as a function of angle θ_1 (as defined in figure 1(a)), relative to that of the isolated sphere, $h_{1,un} = \frac{q_1}{4\pi R^2 \varepsilon_0}(\frac{1}{\varepsilon'} - \frac{1}{\varepsilon})$. (a) $\varepsilon = 80$, $\varepsilon' = 1$, $q_1 = q_2$; (b) $\varepsilon = 1$, $\varepsilon' = 80$, $q_1 = q_2$; (c) $\varepsilon = 80$, $\varepsilon' = 1$, $q_1 = -q_2$; and (d) $\varepsilon = 1$, $\varepsilon' = 80$, $q_1 = -q_2$. Results are shown for three different values of d. Note that the induced charge density is of the same sign as q_1 in (a) and (c) and of the opposite sign in (b) and (d). Identical plots are obtained for sphere 2, but with $\theta_2 = \pi - \theta_1$.

and those in which it is the less polarizable medium ($\varepsilon < \varepsilon'$). The former case could be used to model ions trapped inside water droplets or reverse micelles, surrounded by oil, or inside polarizable pockets within an apolar macromolecule. Here we set $\varepsilon = 80$, representing water, and $\varepsilon' = 1$. In the latter case the model might represent charged residues buried within protein molecules, surrounded by solvent. Here we use $\varepsilon = 1$ and $\varepsilon' = 80$. As noted in [1], it is important to consider both the case of like charges $q_1 = q_2$, and that of unlike charges $q_1 = -q_2$.

3.3.1. Charges at sphere centres. We first position the point charges at the centres of spheres of equal radius $R(\Delta_1 = \Delta_2 = 0)$, and vary their separation d. At very large d, the isolated sphere limit is expected to be recovered, in which a sphere containing a point charge q has a uniform $h(s)$ given by $h_{un} = \frac{q}{4\pi R^2 \varepsilon_0}\left(\frac{1}{\varepsilon'} - \frac{1}{\varepsilon}\right)$. Figure 4 shows that the induced polarization charge density on the two spheres becomes correlated as d is reduced.

When $\varepsilon > \varepsilon'$ ((a) and (c)), the polarization charge on the sphere surface is of the same sign as the point charge within that sphere. In this case, as d decreases, when $q_1 = q_2$ (a), due to repulsion between the like-charged induced charge densities on the two spheres, $h(s)$ becomes depleted in the region where the surfaces are close together (small θ_1, large θ_2). However, when $q_1 = -q_2$ (c), the induced charge densities are of opposite signs and $h(s)$ accumulates in this region.

When $\varepsilon < \varepsilon'$ ((b) and (d)), the polarization charge is of the opposite sign to the charge within the sphere. If $q_1 = q_2$ (b), then once again $h(s)$ is depleted where the spheres are closest (at small θ_2), whereas it accumulates when $q_1 = -q_2$ (d). Correlation effects between the polarization charge densities are far weaker when the medium of high permittivity is outside the spheres than when it is inside.

The function $\varepsilon_{eff}(d)$, defined in equation (4), is plotted in figure 5 for $\varepsilon > \varepsilon'$, $\varepsilon < \varepsilon'$, $q_1 = q_2$, and $q_1 = -q_2$. At large d, ε_{eff} approaches ε'. The behaviour of $\varepsilon_{eff}(d)$ in the four cases can be understood in the context of the correlated polarization surface charge density shown in figure 4. When $\varepsilon > \varepsilon'$ and $q_1 = q_2$ (a), each point charge is repelled not only by the other charge itself, but also by its like-charged polarization surface charge density, $h(s)$. As d decreases, $h(s)$ is depleted in the region between the spheres. This has the effect of reducing the repulsion between the charges, causing ε_{eff} to increase. Putting $\varepsilon < \varepsilon'$ and keeping $q_1 = q_2$ (b), the point charges still experience a bare repulsive interaction, but now the potential due to interaction with $h(s)$ (which now has the opposite charge) is attractive. As d decreases, $h(s)$ is depleted between the spheres, the interaction energy becomes more repulsive, and ε_{eff} decreases. Turning to the situation shown in (c), where $q_1 = -q_2$ and $\varepsilon > \varepsilon'$, each point charge is now attracted to the part of $h(s)$ situated on the other sphere. As d decreases, $h(s)$ accumulates as shown in figure 4 and the attractive potential between the charges is increased, leading to a lower ε_{eff}. Finally, when $q_1 = -q_2$, and $\varepsilon < \varepsilon'$, as shown in (d), each point charge is repelled by the component of $h(s)$ on the opposing sphere. $h(s)$ accumulates between the spheres as d decreases, thereby reducing the attraction between the charges and causing ε_{eff} to increase.

3.3.2. Charges displaced from centre. In a true physical situation, charged objects are sometimes free to move within their containing dielectric bodies. We therefore investigated the effect on the total energy of varying the parameter $\Delta_1 = -\Delta_2 = \Delta$ (see figure 1), which measures the position of the point charges relative to the centres of the spheres. In the limit $d \to \infty$, where the spheres are independent, the energy, given by (17), is nevertheless Δ-dependent. When $\varepsilon > \varepsilon'$, the energy is minimized when the point charge is positioned at the sphere centre, but when $\varepsilon < \varepsilon'$, a location at the sphere boundary is favoured. In the latter case, where, as was noted earlier, interaction effects between the spheres are far weaker, this situation does not change on reducing the separation d. However, in the case when $\varepsilon > \varepsilon'$, setting as before $\varepsilon = 80$ and $\varepsilon' = 1$ and firstly taking $q_1 = q_2$, the minimum in the total energy as a function of Δ is shifted from $\Delta = 0$ as $d \to \infty$ to $\Delta = -0.02$ at $d = 10R$ to $\Delta = -0.20$ at $d = 2.5R$. When $q_1 = -q_2$, the minimum shifts in the other direction, to $\Delta = 0.02$ at $d = 10R$ to $\Delta = 0.31$ at $d = 2.5R$. Thus it is favourable for oppositely charged objects to move towards each other within their polarized surrounding bodies, but for those with the same charge to move away from each other, as the bodies approach one another.

3.3.3. Spheres of different sizes. In this section, we recognize that interacting dielectric bodies containing point charges are not necessarily of equal sizes. Ion-containing water droplets suspended in oil, for instance, are unlikely to be all identical in radius. We therefore investigate the effects on the interaction potential between the charges when one sphere is allowed to be larger than the other.

Figure 6 shows the effect on $\varepsilon_{eff}(d)$ when $R_2 = 2R_1$ and when $R_2 = 4R_1$. It is clear that the correlation between the induced polarization surface charge densities on the two spheres is strongly influenced by the difference in their curvature. Figure 7 shows $h(\theta)/h_{un}$ for the two spheres, for $\varepsilon = 80$, $\varepsilon' = 1$, $q_1 = q_2$, and $R_2 = 2R_1$. As d decreases, the like-

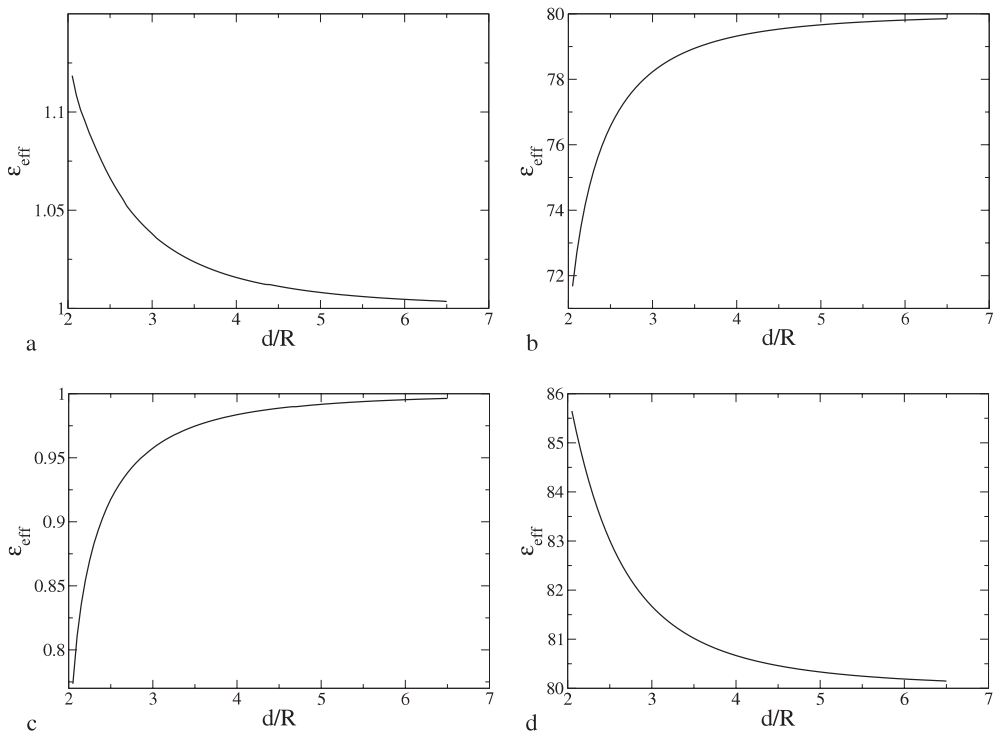

Figure 5. $\varepsilon_{eff}(d)$ in the four cases (a) $\varepsilon = 80, \varepsilon' = 1, q_1 = q_2$; (b) $\varepsilon = 1, \varepsilon' = 80, q_1 = q_2$; (c) $\varepsilon = 80, \varepsilon' = 1, q_1 = -q_2$; and (d) $\varepsilon = 1, \varepsilon' = 80, q_1 = -q_2$.

charged polarization surface charge becomes depleted in the region between the spheres, as in figure 4(a). Moreover, a new effect is present here which is not seen when $R_1 = R_2$. When the spheres are very close together, $h(\theta)$ becomes so depleted on the sphere 2 that it actually changes sign. This reverses its effect on the charge density on sphere 1, which begins to accumulate in this region. This strong correlation between the two spheres is responsible for the dramatic behaviour of $\varepsilon_{eff}(d)$ seen in figure 6.

4. Charges inside a dielectric spheroid

When two dielectric bodies containing charges come very close to one another, they frequently coalesce, creating a single body which contains both charges. This scenario is modelled here by a spheroid with two point charges at its foci, as shown in figure 8.

4.1. Solution in prolate spheroidal coordinates

Using the prolate spheroidal coordinate system [11], an analytical solution of the electrostatic problem is possible. This may be done by the standard method of expanding the electrostatic potential in suitable basis functions and applying the necessary boundary conditions at the dielectric interface [6]. Alternatively, one may expand the induced charge density $h(\boldsymbol{s})$, the Green function $G(\boldsymbol{s} - \boldsymbol{s}')$, and the external potential $\psi_e(\boldsymbol{s})$ in suitable orthogonal basis functions, leading to an expression for the functional $I[h]$ which is easily minimized to yield the expansion coefficients for $h(\boldsymbol{s})$.

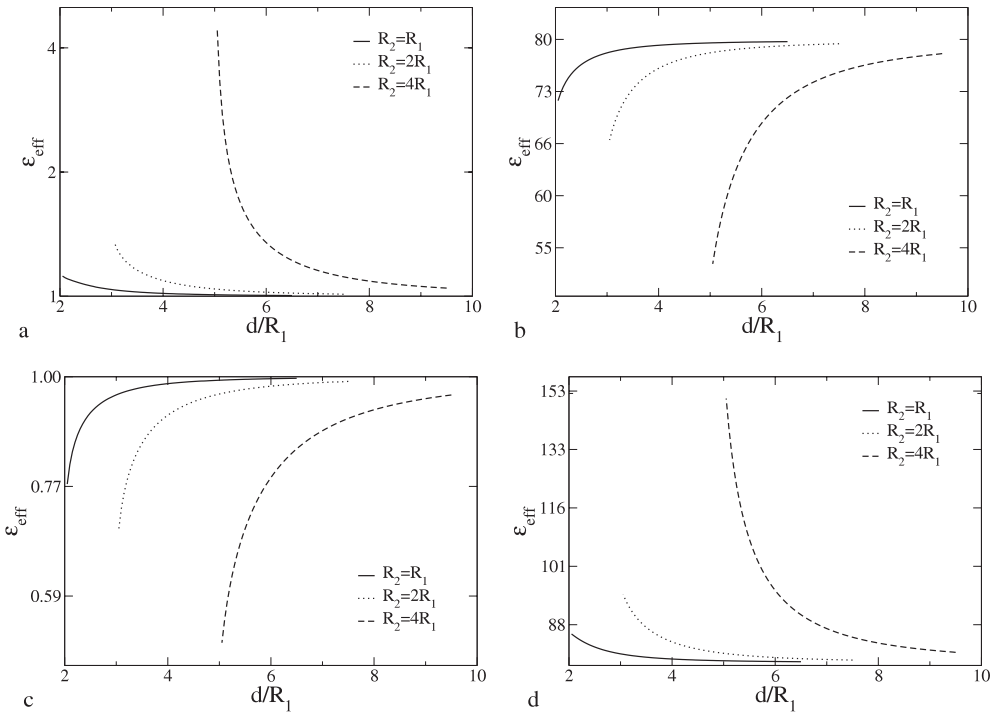

Figure 6. $\varepsilon_{eff}(d)$ for $R_2 = R_1$, $R_2 = 2R_1$, and $R_2 = 4R_1$, in the four cases (a)–(d), labelled as in figures 4 and 5. Note that the scale on the y-axis is logarithmic.

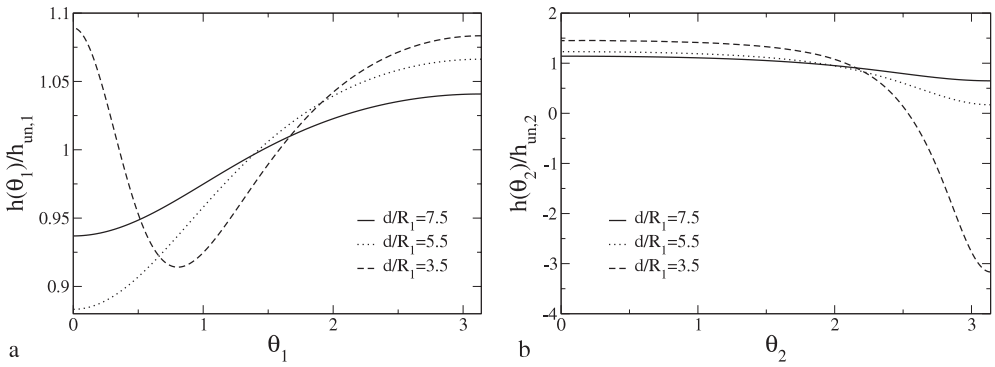

Figure 7. Induced polarization charge density on sphere 1 (a), and on sphere 2 (b), relative to its value on the same sphere as $d \to \infty$. $R_1 = 2R_2$, $\varepsilon = 80$, $\varepsilon' = 1$, and $q_1 = q_2$. Results are shown for three different values of d.

In prolate spheroidal coordinates (ζ, η, ϕ), the surfaces $\zeta = \zeta_0$ are prolate spheroids with major axis $a\zeta/2$ and foci at $z = \pm a/2$. The ϕ-coordinate is the azimuthal angle. Positions on the surface of the spheroid are described in terms of η, where $z = a\eta\zeta/2$. The solution, as described in appendix B, leads to a series expansion of $h(\boldsymbol{s})$:

$$h(\eta) = \sum_{n=0}^{\infty} C_n \frac{P_n(\eta)}{\sqrt{(\zeta_0^2 - \eta^2)}} \tag{20}$$

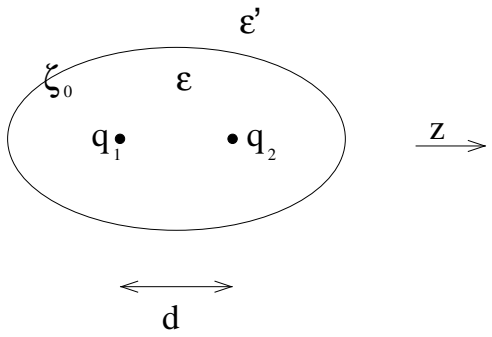

Figure 8. An illustration of the geometry of the problem in prolate spheroidal coordinates.

where the coefficients C_n, determined by minimization of the functional $I[h]$, are given in equation (B.8).

The polarization energy is given by expression (B.9). From this, the total energy is obtained using (15). For the problem of two charges inside separate spheres, the interaction energy was defined in (16), subtracting from the total energy the polarization energy at large sphere separation. However, in the present geometry, such a subtraction is not appropriate and we define the corresponding effective dielectric function $\mathcal{E}_{eff}(d)$ by

$$V_{tot}(d) = \frac{q_1 q_2}{4\pi \mathcal{E}_{eff} \varepsilon_0 d}. \tag{21}$$

In performing these calculations, it is necessary to choose an appropriate size of spheroid for each value of d. We have here taken the dielectric medium containing the point charges to be incompressible, and maintained the total volume of the spheroid at the same value as that of two isolated spheres of radius R. This amounts to calculating the parameter ζ_0 from the relation

$$\frac{\pi a^3 \zeta_0}{6}(\zeta_0^2 - 1) = \frac{8\pi R^3}{3}. \tag{22}$$

The value of a is set by the distance between the point charges, $a = d$.

4.2. Results

The effective dielectric function $\mathcal{E}_{eff}(d)$ is plotted in figure 9 for $\varepsilon > \varepsilon'$, $\varepsilon < \varepsilon'$, $q_1 = q_2$, and $q_1 = -q_2$. In all cases, when the two point charges are very close, $d \to 0$, the second part of equation (15) dominates and $\mathcal{E}_{eff} \to \varepsilon$. For larger values of d, the polarization of the surrounding spheroid comes into play. The relative influence of E_{pol} increases with d, since the charges move apart from each other but become closer to the dielectric boundary. If $\varepsilon > \varepsilon'$, each point charge induces polarization charge of the same sign on the surface closest to it, giving a repulsive polarization energy, E_{pol}. When $q_1 = q_2$ (a), E_{pol} adds to the repulsive second term in (15), causing $\mathcal{E}_{eff}$ to decrease as d increases. When $q_1 = -q_2$ (c), E_{pol} opposes the attractive second term in (15), reducing the effective attraction between the charges. Thus $\mathcal{E}_{eff}$ increases. At $d/R \approx 1.25$, the two terms in (15) exactly cancel, giving $E_{tot} = 0$ and a divergence in $\mathcal{E}_{eff}$. When $d/R > 1.25$, the polarization term dominates and $\mathcal{E}_{eff}$ is negative. On the other hand, if $\varepsilon < \varepsilon'$, each point charge induces polarization charge around it of opposite sign, leading to a negative E_{pol}. Thus the attractive second term in (15) when $q_1 = q_2$ is opposed and eventually overcome by E_{pol}, causing $\mathcal{E}_{eff}$ to increase, diverge and become negative in (b).

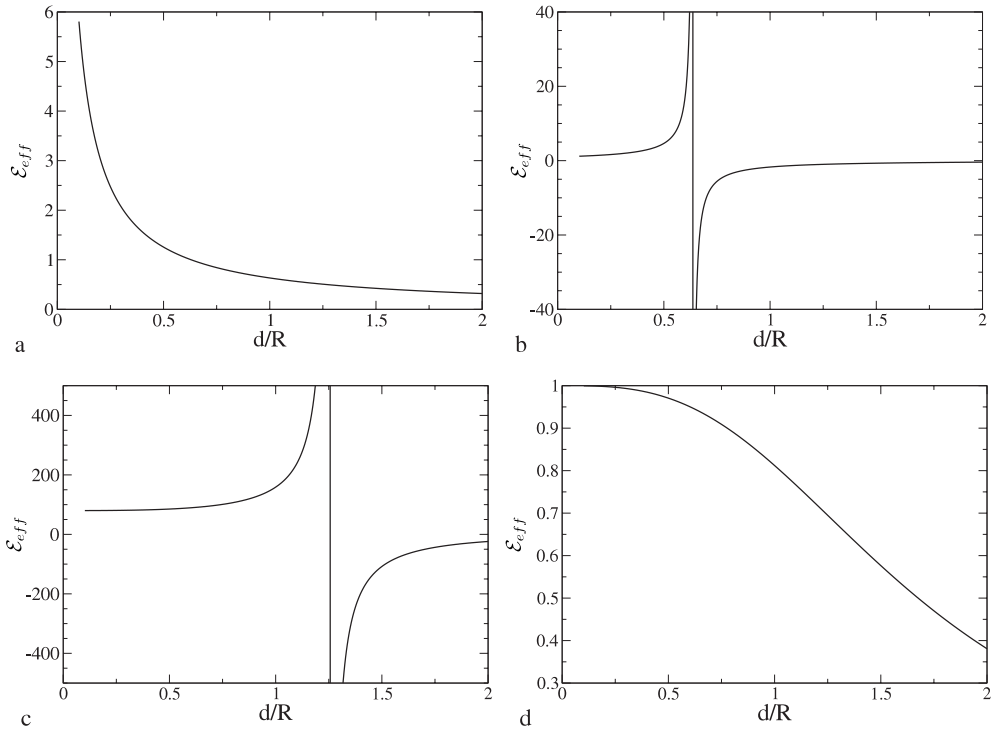

Figure 9. $\mathcal{E}_{eff}(d)$, as defined in (21), for the four cases (a)–(d), labelled as in figures 4–6.

However, when $q_1 = -q_2$, the effect of the negative E_{pol} is to reinforce the negative second term, decreasing $\mathcal{E}_{eff}$ (d). Divergences in effective dielectric functions were also observed by Ehrenson [12] in a different context. This seemingly unphysical behaviour may in fact be traced back to the somewhat arbitrary definition of a bulk-like dielectric constant in confined geometries.

5. Conclusions

Phenomenological, distance-dependent dielectric functions are frequently employed in continuum descriptions of solvents near interfaces. A much studied biophysical application is that of the solvation of macromolecules such as proteins and DNA [13]; however, the form of the distance dependence of the dielectric function is mostly *ad hoc*. In the present paper we have investigated the possibility of defining a distance-dependent dielectric constant $\varepsilon(d)$ from a purely macroscopic point of view, based on the classical theory of dielectrics and the assumption of infinitely sharp interfaces.

The analytical and numerical results show that $\varepsilon(d)$ is meaningful in the case of charges embedded inside non-intersecting spheres. A very significant increase or decrease of $\varepsilon(d)$ relative to its asymptotic value ε' is found for spheres close to contact ($d \gtrsim 2R$), depending on the relative sign of the two charges and the relative values of the dielectric constants inside and outside the spheres. The most important conclusion is that different effective dielectric constants must be defined for interactions between equal and opposite charges. The increase or reduction of $\varepsilon(d)$ relative to ε' for small d is considerably enhanced when the embedding spheres have different radii.

Very different results are found when the two charges are embedded within the same spheroidal cavity, but the concept of a distance-dependent dielectric function is less clear in that case; our variational method gives similar results to earlier work by Westheimer and Kirkwood [6] using different methods. The present approach is being generalized to the case of three spherical bodies, to investigate the importance of three-body interactions, and to charges interacting through a dielectric slab representing a membrane.

Acknowledgments

The authors would like to thank Professor R Lynden-Bell for providing the motivation for this work, R Finken for his help with the solution in bispherical coordinates, and A J Stone for his assistance with spherical harmonics. RA is grateful to EPSRC for funding and to Unilever for a CASE award.

Appendix A. Solution of the two-sphere problem in bispherical coordinates

Using the bispherical coordinate system (μ, η, ϕ) [11], the external potential due to point charges q_1, situated on the z-axis at $z = -a$, and q_2 at $z = +a$, is given by

$$\psi_e = \frac{1}{4\sqrt{2}\pi\varepsilon\varepsilon_0 a}\sqrt{(\cosh\mu - \cos\eta)}(q_1 e^{-\mu/2} + q_2 e^{\mu/2}). \tag{A.1}$$

The total electrostatic potential is given in the three regions 1, 2, and 3, as shown in figure 2, by

$$\begin{aligned}
\psi_1 &= \psi_e + \sum_n A_n\sqrt{(\cosh\mu - \cos\eta)}e^{(n+\frac{1}{2})\mu}P_n(\cos\eta)\\
\psi_2 &= \psi_e + \sum_n \sqrt{(\cosh\mu - \cos\eta)}[B_n e^{(n+\frac{1}{2})\mu} + C_n e^{-(n+\frac{1}{2})\mu}]P_n(\cos\eta)\\
\psi_3 &= \psi_e + \sum_n D_n\sqrt{(\cosh\mu - \cos\eta)}e^{-(n+\frac{1}{2})\mu}P_n(\cos\eta)
\end{aligned} \tag{A.2}$$

where the coefficients A_n, B_n, C_n, and D_n are to be determined.

The component of the electric field $\boldsymbol{E} = -\boldsymbol{\nabla}\psi$, in the $\boldsymbol{e}_\mu$-direction, can be shown to be

$$E_\mu = -\frac{(\cosh\mu - \cos\eta)}{a}\frac{\partial\psi}{\partial\mu}. \tag{A.3}$$

The boundary conditions on the electrostatic potential at the dielectric interfaces, $\mu = \mu_0$ and $\mu = -\mu_0$, are

$$\begin{aligned}
&\psi_1|_{-\mu_0} = \psi_2|_{-\mu_0}; \qquad \varepsilon\frac{\partial\psi_1}{\partial\mu}\bigg|_{-\mu_0} = \varepsilon'\frac{\partial\psi_2}{\partial\mu}\bigg|_{-\mu_0};\\
&\psi_3|_{\mu_0} = \psi_2|_{\mu_0}; \qquad \varepsilon\frac{\partial\psi_3}{\partial\mu}\bigg|_{\mu_0} = \varepsilon'\frac{\partial\psi_2}{\partial\mu}\bigg|_{\mu_0}.
\end{aligned} \tag{A.4}$$

Applying (A.4) to (A.2), using the recursion relations for Legendre polynomials [14], and equating coefficients of $P_n(\cos\eta)$, one obtains a set of coupled equations for the coefficients:

$$A_n = B_n + C_n e^{(2n+1)\mu_0} \tag{A.5}$$

$$D_n = C_n + B_n e^{(2n+1)\mu_0} \tag{A.6}$$

$$\begin{aligned}
&\varepsilon A_n(\alpha_n e^{\mu_0} + \gamma_n e^{-\mu_0}) - \varepsilon\gamma_{n-1}A_{n-1} - \varepsilon\alpha_{n+1}A_{n+1}\\
&\quad - \varepsilon' B_n(\alpha_n e^{\mu_0} + \gamma_n e^{-\mu_0}) + \varepsilon'\gamma_{n-1}B_{n-1} + \varepsilon'\alpha_{n+1}B_{n+1}\\
&\quad + \varepsilon' C_n(\delta_n e^{\mu_0} + \beta_n e^{-\mu_0}) - \varepsilon'\delta_{n-1}C_{n-1} - \varepsilon'\beta_{n+1}C_{n+1} = X_n
\end{aligned} \tag{A.7}$$

$$-\varepsilon D_n(\alpha_n e^{\mu_0} + \gamma_n e^{-\mu_0}) + \varepsilon\gamma_{n-1}D_{n-1} + \varepsilon\alpha_{n+1}D_{n+1} - \varepsilon' B_n(\delta_n e^{\mu_0} + \beta_n e^{-\mu_0}) + \varepsilon'\delta_{n-1}B_{n-1} + \varepsilon'\beta_{n+1}B_{n+1} + \varepsilon' C_n(\gamma_n e^{-\mu_0} + \alpha_n e^{\mu_0}) - \varepsilon'\gamma_{n-1}C_{n-1} - \varepsilon'\alpha_{n+1}C_{n+1} = Y_n. \tag{A.8}$$

Here, X_n and Y_n are given by

$$X_n = \begin{cases} \dfrac{(\varepsilon' - \varepsilon)}{4\sqrt{2}\pi\varepsilon a}[-q_1 e^{\frac{3}{2}\mu_0} + q_2 e^{-\frac{3}{2}\mu_0}] & (n = 0) \\ \dfrac{(\varepsilon' - \varepsilon)}{4\sqrt{2}\pi\varepsilon a}[q_1 e^{\frac{1}{2}\mu_0} - q_2 e^{-\frac{1}{2}\mu_0}] & (n = 1) \\ 0 & (n > 1) \end{cases} \tag{A.9}$$

$$Y_n = \begin{cases} \dfrac{(\varepsilon' - \varepsilon)}{4\sqrt{2}\pi\varepsilon a}[-q_1 e^{-\frac{3}{2}\mu_0} + q_2 e^{\frac{3}{2}\mu_0}] & (n = 0) \\ \dfrac{(\varepsilon' - \varepsilon)}{4\sqrt{2}\pi\varepsilon a}[q_1 e^{-\frac{1}{2}\mu_0} - q_2 e^{\frac{1}{2}\mu_0}] & (n = 1) \\ 0 & (n > 1) \end{cases} \tag{A.10}$$

and α_n, β_n, γ_n, and δ_n by

$$\begin{aligned} \alpha_n &= n e^{-(n+\frac{1}{2})\mu_0} & \gamma_n &= (n+1)e^{-(n+\frac{1}{2})\mu_0} \\ \beta_n &= n e^{(n+\frac{1}{2})\mu_0} & \delta_n &= (n+1)e^{(n+\frac{1}{2})\mu_0}. \end{aligned} \tag{A.11}$$

Substituting equations (A.5) and (A.6) into (A.7) and (A.8), we obtain linear equations for B_n and C_n:

$$(\varepsilon' - \varepsilon)\alpha_{n+1}B_{n+1} - (\varepsilon + \varepsilon')\beta_{n+1}C_{n+1} - (\varepsilon' - \varepsilon)[\gamma_n e^{-\mu_0} - \alpha_n e^{\mu_0}]B_n + [\delta_n(\varepsilon e^{-\mu_0} + \varepsilon' e^{\mu_0}) + \beta_n(\varepsilon e^{\mu_0} + \varepsilon' e^{-\mu_0})]C_n + (\varepsilon' - \varepsilon)\gamma_{n-1}B_{n-1} - (\varepsilon + \varepsilon')\delta_{n-1}C_{n-1} = X_n \tag{A.12}$$

$$-(\varepsilon' - \varepsilon)\alpha_{n+1}C_{n+1} + (\varepsilon + \varepsilon')\beta_{n+1}B_{n+1} + (\varepsilon' - \varepsilon)[\gamma_n e^{-\mu_0} + \alpha_n e^{\mu_0}]C_n - [\delta_n(\varepsilon e^{-\mu_0} + \varepsilon' e^{\mu_0}) + \beta_n(\varepsilon e^{\mu_0} + \varepsilon' e^{-\mu_0})]B_n - (\varepsilon' - \varepsilon)\gamma_{n-1}C_{n-1} + (\varepsilon + \varepsilon')\delta_{n-1}B_{n-1} = Y_n. \tag{A.13}$$

When $n = 0$, the coefficients A_{n-1}, B_{n-1}, C_{n-1}, and D_{n-1} in this set of equations are all defined to be zero.

Equations (A.12) and (A.13) are solved using a standard linear equation solver, with the series being truncated after a finite number of coefficients N; $N \approx 10$ is usually sufficient to converge the induced polarization surface charge density. Equations (A.5) and (A.6) then allow the remaining coefficients A_n and D_n to be calculated.

The induced polarization surface charge density is obtained from the discontinuity in the electric field component E_μ at the surfaces $\mu = \pm\mu_0$ [7]:

$$h^{(1)}(\eta) = E_\mu^{(2)}(-\mu_0) - E_\mu^{(1)}(-\mu_0) = -\frac{(\cosh\mu - \cos\eta)}{a}\frac{\partial}{\partial\mu}[\psi_2 - \psi_1]_{\mu=-\mu_0} \tag{A.14}$$

$$h^{(2)}(\eta) = E_\mu^{(3)}(\mu_0) - E_\mu^{(2)}(\mu_0) = -\frac{(\cosh\mu - \cos\eta)}{a}\frac{\partial}{\partial\mu}[\psi_3 - \psi_2]_{\mu=\mu_0}. \tag{A.15}$$

Applying relations (A.14) and (A.15) to (A.2) and once more using the Legendre polynomial recursion relation, one arrives at an induced charge density of the form given in equations (18) and (19), where the coefficients Z_n and W_n are given by

$$Z_n = -\frac{1}{2a}[(B_n - A_n)(\gamma_n e^{-\mu_0} + \alpha_n e^{\mu_0}) - (B_{n-1} - A_{n-1})\gamma_{n-1} - (B_{n+1} - A_{n+1})\alpha_{n+1} - C_n(\beta_n e^{-\mu_0} + \delta_n e^{\mu_0}) + C_{n-1}\delta_{n-1} + C_{n+1}\beta_{n+1}] \quad (A.16)$$

$$W_n = -\frac{1}{2a}[-(D_n - C_n)(\alpha_n e^{\mu_0} + \gamma_n e^{-\mu_0}) + (D_{n-1} - C_{n-1})\gamma_{n-1} + (D_{n+1} - C_{n+1})\alpha_{n+1} - B_n(\beta_n e^{-\mu_0} + \delta_n e^{\mu_0}) + B_{n-1}\delta_{n-1} + B_{n+1}\beta_{n+1}]. \quad (A.17)$$

The resulting functions (18) and (19) are plotted in figure 3 and compared to the results of the numerical procedure described in section 3.1.

Appendix B. Solution of the prolate spheroid problem

The external potential due to two point charges, q_1 and q_2, situated at $z = \pm a/2$, as shown in figure 8, is

$$\psi_e(\zeta, \eta) = \frac{1}{2\pi a \varepsilon \varepsilon_0} \sum_{n=0}^{\infty} (2n+1) P_n(\eta) Q_n(\zeta)[(-1)^n q_1 + q_2]. \quad (B.1)$$

The surface polarization charge density $h(\boldsymbol{s})$ is expanded as in (20). The Green function is given by

$$G(\boldsymbol{r} - \boldsymbol{r}') = \frac{1}{4\pi|\boldsymbol{r} - \boldsymbol{r}'|} = \frac{1}{2\pi a} \sum_{n=0}^{\infty} (2n+1) \sum_{m=0}^{n} \varepsilon_m \mathrm{i}^m \left[\frac{(n-m)!}{(n+m)!}\right]^2 \times \cos(m(\phi - \phi')) P_n^m(\eta) P_n^m(\eta') P_n^m(\zeta_<) Q_n^m(\zeta_>) \quad (B.2)$$

where $P_n^m(x)$ and $Q_n^m(x)$ are associated Legendre functions of the first and second kinds. The normal derivative to the surface $\zeta = \zeta_0$ is given by [15]

$$\frac{\partial}{\partial n} = \frac{2}{a}\left(\frac{\zeta^2 - 1}{\zeta^2 - \eta^2}\right)^{1/2} \left.\frac{\partial}{\partial \zeta}\right|_{\zeta = \zeta_0} \quad (B.3)$$

and integrations over that surface are performed using the relation [15]

$$\int \mathrm{d}^2 s = \frac{a^2}{4}(\zeta_0^2 - 1)^{1/2} \int_{-1}^{1} \mathrm{d}\eta\, (\zeta_0^2 - \eta^2)^{1/2} \int_0^{2\pi} \mathrm{d}\phi. \quad (B.4)$$

Substituting (B.1), (20), (B.2)–(B.4) into the functional (2) and exploiting the orthogonality relations for trigonometric and Legendre functions, we obtain the result

$$I[h] = \sum_{n=0}^{\infty} I_n(C_n) \quad (B.5)$$

where

$$\frac{8 I_n}{(\zeta_0^2 - 1)^{3/2} a Q_n(\zeta_0)} = [(-1)^n q_1 + q_2] \times C_n \frac{(\kappa - 1)}{\varepsilon \varepsilon_0}[(\zeta_0^2 - 1)^{-1} - 3P_n(\zeta_0)Q_n'(\zeta_0) - P_n'(\zeta_0)Q_n(\zeta_0)] + \frac{a^2 \pi (\zeta_0^2 - 1)^{1/2} C_n^2 P_n(\zeta_0)}{(2n+1)}[(\kappa + 1)(\zeta_0^2 - 1)^{-1} - (\kappa - 1)[P_n(\zeta_0)Q_n'(\zeta_0) + P_n'(\zeta_0)Q_n(\zeta_0)]]. \quad (B.6)$$

Using the relation [14]

$$P_n'(\zeta_0)Q_n(\zeta_0) - P_n(\zeta_0)Q_n'(\zeta_0) = (\zeta_0^2 - 1)^{-1} \quad (B.7)$$

and setting $\frac{dI^{(n)}}{dC_n} = 0$, allows an expression for the coefficients C_n to be obtained:

$$C_n = \frac{(2n+1)[(-1)^n q_1 + q_2]Q_n'(\zeta_0)(1-\kappa)}{\varepsilon\varepsilon_0 a^2\pi\sqrt{\zeta_0^2-1}[\kappa P_n(\zeta_0)Q_n'(\zeta_0) - P_n'(\zeta_0)Q_n(\zeta_0)]}. \tag{B.8}$$

It is easily verified that the total induced surface charge, given by $Q = \varepsilon_0 a^2 \pi C_0$, is the correct value, $Q = (q_1 + q_2)(\varepsilon - \varepsilon')/(\varepsilon\varepsilon')$. The polarization energy is calculated using (14), leading to the result

$$V_{pol} = -\sum_{n=0}^{\infty} \frac{(\varepsilon' - \varepsilon)Q_n(\zeta_0)Q_n'(\zeta_0)(2n+1)((-1)^n q_1 + q_2)^2}{4\varepsilon\varepsilon_0\pi a[\varepsilon' P_n(\zeta_0)Q_n'(\zeta_0) - \varepsilon P_n'(\zeta_0)Q_n(\zeta_0)]}. \tag{B.9}$$

References

[1] Ha Duong T, Phan S, Marchi M and Borgis D 2002 *J. Chem. Phys.* **117** 541
[2] Marchi M, Borgis D, Levy N and Ballone P 2001 *J. Chem. Phys.* **114** 4377
[3] York D M and Karplus M 1999 *J. Phys. Chem.* A **103** 11 060
[4] Allen R, Melchionna S and Hansen J-P 2002 *Preprint* cond-mat/0205454
[5] Allen R, Hansen J-P and Melchionna S 2001 *Phys. Chem. Chem. Phys.* **3** 4177
[6] Westheimer F H and Kirkwood J G 1938 *J. Chem. Phys.* **6** 513
[7] Jackson J D 1999 *Classical Electrodynamics* 3rd edn (New York: Wiley)
[8] Varshalovich D A, Moskalev A N and Khersonskii V K 1988 *Quantum Theory of Angular Momentum* (Singapore: World Scientific)
[9] Brink D M and Satchler G R 1968 *Angular Momentum* (Oxford: Clarendon)
[10] Press W H, Teukolsky S A, Vetterling W T and Flannery B P 1992 *Numerical Recipes in Fortran* (Cambridge: Cambridge University Press)
[11] Morse P M and Feshbach H 1953 *Methods of Theoretical Physics* (New York: McGraw-Hill)
[12] Ehrenson S 1982 *J. Am. Chem. Soc.* **104** 4793
[13] See, e.g.,
Schaefer M, Bartels C and Karplus M 1999 *Theor. Chem. Acc.* **101** 194
[14] Abramowitz M and Stegun I A 1972 *Handbook of Mathematical Functions* (New York: Dover)
[15] Arfken G B and Weber H J 1995 *Mathematical Methods for Physicists* 4th edn (New York: Academic)